

Leaky Frontends: Micro-Op Cache and Processor Frontend Vulnerabilities

Shuwen Deng, Bowen Huang, and Jakub Szefer
Yale University
{shuwen.deng, bowen.huang, jakub.szefer}@yale.edu

Abstract—This paper demonstrates a new class of security vulnerabilities due to the Micro-Op Caches, also called Decode Stream Buffer, and other components in the processor frontend. The vulnerabilities presented in this work exploit multiple paths in the processor frontend that the micro-ops can take: through the Micro-Instruction Translation Engine (MITE), through the Decode Stream Buffer (DSB), or through the Loop Stream Detector (LSD). Each path has its own unique timing and power signature, which leads to security vulnerabilities. The vulnerabilities can be used as side or covert channels for information leakage and can be exploited to create both timing and power attacks. As information leakage channels, the new vulnerabilities are orthogonal to the existing speculative execution attacks and can be used as covert transmission channels in a new variant of speculative attacks that is demonstrated in this work. The vulnerabilities further affect Intel SGX enclaves, and this work shows how information can be leaked from SGX enclaves through the sharing of the frontend paths. The transmission rates for new attacks based on the vulnerabilities presented can be as high as 1410 Kbps (1.41 Mbps) with an almost 0% error rate. Consequently, this work demonstrates that multiple paths in the processor frontend are a source of security vulnerabilities which have not been considered before and that focusing on just speculative execution attacks is not sufficient to secure today’s processors.

I. INTRODUCTION

The processor frontend is responsible for fetching, decoding and delivering instructions to the rest of the processor pipeline. To enhance performance and reduce power, multiple paths for instruction decoding and delivery are widely adopted in today’s processor designs. The frontend has become complex in modern processors, with multiple structures used to assist in the effective decoding and delivery of the micro-ops [1].

The processor frontend is designed to ideally not become a bottleneck, so that the backend is always fed with sufficient instructions to process. Consequently, majority of timing or power variations that can be observed in processors are due to components in the backend as that is the bottleneck where execution differences can be more easily observed – and this has resulted in various security vulnerabilities that have been previously uncovered [4], [14], [16], [21], [40]. Meanwhile, this is the first work to extensively evaluate the security of the processor frontend paths. In particular, we are the first to observe that there are multiple instruction decoding and delivery paths in the frontend, leading to new vulnerabilities resulting in timing and power attacks. The paths include the Micro-Instruction Translation Engine (MITE), the Decoded

Stream Buffer (DSB), also called the micro-op cache, and the Loop Stream Detector (LSD).

Instruction decoding and delivery was previously achieved by MITE within the pipeline [1], but it incurs high power and creates performance overhead. Therefore, the DSB and LSD were introduced starting from Intel Core microarchitectures to improve performance and power. As the result, in today’s processors, the same instruction can possibly go through 1 out of 3 different paths: MITE, DSB, or LSD. These paths are invisible at the instruction set architecture level, but do have unique timing and power signatures at the microarchitecture level. The different paths are basis of the vulnerabilities that we demonstrate. The vulnerabilities are different and independent from speculative attacks [5], [7], [18], [20], [29], [31], branch predictor attacks [10], [11], or processor backend attacks [4], [16], [21], [40]. *Consequently, this work demonstrates that focusing on just the speculative attacks is not sufficient to secure today’s processors, as frontend is a source of security vulnerabilities that need to be mitigated as well.*

Most of the existing architecture security studies have focused on the processor backend and the out-of-order execution engine. Security vulnerabilities have been uncovered which are caused by all the different levels of caches [4], [16], [21], [40], port contention in the execution engine [3], branch predictors [10], [11], or memory controllers [35], for example. Security community has especially focused on the speculative execution attacks, following Spectre [5], [7], [18], [29], Meltdown [7], [20], Foreshadow [32], [36], and various Microarchitectural Data Sampling [6], [28], [33], [34] attacks. The root-cause of these speculative attacks is that the processor speculatively executes certain instructions and either does not properly clean up the microarchitectural state, or allows certain data to be accessed during speculative execution without proper authorization or checks [38]. All these attacks happen after the instructions have already been decoded.

Meanwhile, the instruction decoding in the processor frontend has a unique feature where the same instruction decoding and delivery of micro-ops can take different paths. This has important implications: each instruction (or its decoded micro-ops) can be concurrently located in up to three structures: MITE, DSB, and LSD. The execution timing and power depend on the exact path taken in the frontend. The three paths are the sources of the new vulnerabilities this work presents.

The different paths lead to different execution timing based on how the instructions are handled by the MITE, DSB, or LSD. Timing can be measured by unprivileged attackers

running on the same core in the same or different threads. Further, the power-based information leakage is fully observed in software by an attacker that accesses energy counters, e.g., Intel’s Running Average Power Limit (RAPL) [1], available in today’s processors. We also demonstrate that the vulnerabilities can be used against Intel SGX enclaves. And they can also be used as covert channels in a new variant of Spectre that we demonstrate.

The vulnerabilities encompass a number of attacks which are all derived from the multiple paths in the frontend. Our multi-threaded (SMT) attacks use different threads for the sender and the receiver, and leverage evictions or misalignments in DSB or LSD (which are shared by the hardware threads) to create different timing or power variations that can be measured by the receiver. Each attack can further be broken down into a faster, but less stealthy attacks, or slower but more stealthy attacks. For all the attacks, the attacks only affect the frontend and do not, for example, cause interference in the L1 instruction (L1I) caches. The multi-threaded attacks can further be applied to attack SGX enclaves. We also present attacks that do not require multi-threading and mainly use internal-interference among the sender’s own code to cause timing or power variations that the attacker can measure. The non-SMT attacks can be applied to SGX or as a new in-domain Spectre attack.

Having presented new microarchitectural vulnerabilities, the paper also discuss challenges for how to mitigate them, and brings to attention that different paths in the processor frontend, which have not been studied in detail before, are new security threats.

A. Contributions

The contributions of this paper are:

- The first detailed security analysis of the architecture of the processor frontend in modern Intel processors, considering the Micro Instruction Translation Engine (MITE), the Decoded Stream Buffer (DSB), and the Loop Stream Detector (LSD); including reconstructing the part of the address mapping (hash) function needed to map virtual addresses to the same DSB sets.
- The design and proof-of-concept implementation of new frontend attacks, a new class of covert-channel attacks that abuse the MITE, DSB, or LSD to leak information.
 - Design of covert channels making use of contention and misalignment of DSB and LSD entries.
 - Development of frontend attacks which can covertly send bits between hyper-threads or on the same thread in time-sliced setting using internal-interference.
 - Design of both timing-based and power-based variants of the attacks.
- Demonstration of the frontend attacks’ ability to leak information from Intel SGX enclaves.
- Demonstration of the use of the frontend covert-channels as part of a new Spectre attack variant.

B. Responsible Disclosure

Our research findings and copy of this paper have been shared with Intel.

II. BACKGROUND

Various microarchitectural optimizations have emerged in past years as sources of security vulnerabilities, with majority of recent work focusing on speculative execution attacks [38]. Meanwhile, speculative execution is not the only class of vulnerabilities that can affect processors. In this section, we present brief background on various microarchitecture-related security vulnerabilities, and place our new vulnerabilities in context of other known vulnerability types.

There are today numerous variants of speculative execution beyond the main Spectre [18], Meltdown [20], and Microarchitectural Data Sampling (MDS) attacks, e.g., the recent Snoop [2] or LVI [33] attacks. Other recently explored vulnerabilities include attacks that abuse branch prediction, but not for Spectre-like attacks. This includes BranchScope vulnerability [11] or Jump over ASLR type vulnerabilities [10]. Further, certain vulnerabilities abuse the fact that some operations cause exception to trigger handling them in software, e.g., subnormal floating-point operations may cause exception so they can be performed in software [12], leading to execution timing variations. There are also attacks that leverage prefetchers [15] and other predictors [9]. There are also many cache related vulnerabilities, e.g., [4], [16], [21], [40]. Port contention attacks also exist [3]. Most recently, researchers have also demonstrated microarchitectural replay attacks [30] and attacks abusing network-on-chip (NoC) [25].

The vulnerabilities that we present are a new type of vulnerabilities that we derive from the behavior of the instruction decoding logic in the processor frontend, and are different from all previous types of vulnerabilities. Especially, they are orthogonal to speculative execution attacks.

A. Threat Model and Assumptions

This paper focuses on analyzing security considering remote attacks, such as when the victim and the attacker are co-located on the same server, but attacker does not have physical access to the machine. We assume there is one sender (victim) that holds security-critical information and one receiver (attacker) that tries to extract the secret information by measuring timing and power changes. We demonstrate vulnerabilities in both hyper-threading setting (Section IV-A and IV-B) where the two are run in different hardware threads sharing the same core, and attacks in single-threaded setting where the victim and the attacker are time-sharing the code. The single-threaded attacks mainly leverage internal-interference among the sender’s own code (Section IV-C) to cause timing or power variations that the attacker can measure. The timing-based attacks can be performed fully from the user level privilege. The power channels require access on Linux to Intel’s RAPL [1] to extract energy information.

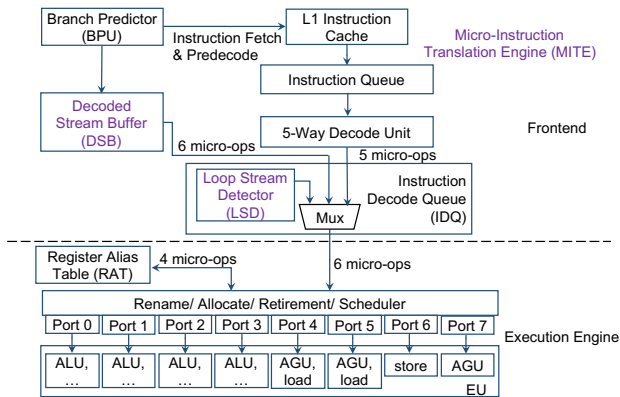


Fig. 1: Microarchitecture details of frontend and execution engine.

III. ANALYSIS OF FRONTEND MICROARCHITECTURE OPERATION

Within the processor frontend, instruction decoding and delivery to the backend has multiple paths: the Micro-Instruction Translation Engine (MITE), the Decoded Stream Buffer (DSB), also called the micro-op cache, and the Loop Stream Detector (LSD), as is seen from Figure 1. Instruction decoding and delivery were originally achieved by MITE [1], which is essentially the x86 legacy decode pipeline. Decoded micro-ops from MITE would be stored into the instruction decode queue (IDQ), which serves as the boundary between the frontend and the backend.

Given that MITE path has low throughput and high power consumption, the DSB has been added and the micro-ops decoded by MITE are inserted into the DSB [1] in modern Intel processors. If the micro-ops are available in the DSB, the micro-op stream is sent directly from DSB to the IDQ, bypassing the MITE, therefore saving power and improving throughput. The instruction delivery path from DSB is also shorter than MITE (shorter by 2 – 4 cycles), so the pipeline latency is reduced as well.

Further, there is also the LSD located within the IDQ. If the micro-op stream belongs to a qualified loop (discussed in Section III-A4), then all the micro-ops belonging to the loop code can be issued directly from LSD to the backend, bypassing DSB as well. The purpose of the LSD is mainly to help save power. When branch mis-prediction occurs, for example at the end of the loop, or the number of micro-ops within the loop exceeds the limit that the LSD can handle, LSD is not used and micro-ops are delivered from the DSB. Furthermore, if the micro-ops exceed the DSB limit or belong to a newly accessed micro-ops, they are processed by the MITE.

As can be seen from Figure 1, the same instruction can then possibly go through any 1 out of the 3 different paths (MITE, DSB, or LSD). These paths have different instruction delivery bandwidth, so they produce timing differences that, as we show, can be abused to leak information. Moreover, depending on which path in the frontend is taken and which units (MITE, DSB, or LSD) are utilized, different amounts of power are used. In this paper, we describe a set of new security

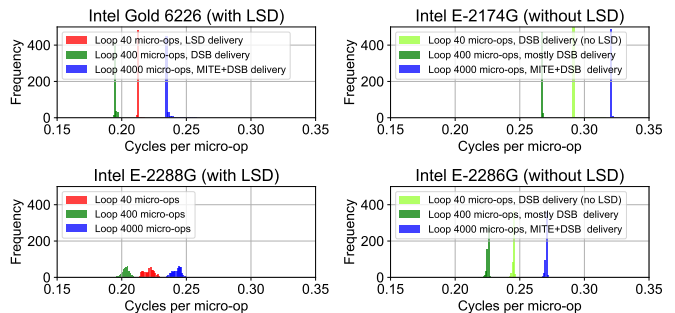


Fig. 2: Histograms showing cycles per micro-op depending on the number of micro-ops within a loop (average cycles per micro-op is smaller than 1 because processor can handle multiple instructions in parallel). Small loops fit in the LSB (red), medium-size loops do not fit in LSB but can be serviced by the DSB (green), while large loops are processed by MITE and DSB as they exceed DSB size limit (blue). Intel E-2288G processor’s performance counters related to the frontend are disabled so we cannot confirm which loop size triggers LSD, DSB, or MITE; but using available cycle counters we see patterns similar to other processors.

threats associated with different timing and power signatures of the frontend paths.

A. Controlling Use of the Frontend Paths

In this section we discuss how the states of the frontend components can be set to achieve execution through the different frontend paths.

1) *Controlling How LSD is Used:* The LSD can continuously stream the same sequence of up to 64 micro-ops, directly from the IDQ to the backend [1], as is shown in Figure 1. While the LSD is active, the rest of the frontend is effectively disabled. In order to generate detectable timing and power difference between LSD vs. DSB and DSB vs. MITE, one can control the number of micro-ops within a loop to either make it fit in the LSD, so that instruction delivery starts with LSD only, or to exceed the LSD limit so the processor falls back to using DSB or MITE, creating timing and power differences that can be detected.

2) *Controlling How DSB is Used:* The DSB is constructed as a cache-like structure with 32 sets and 8 ways per set. Each line can store up to 6 micro-ops or 32 bytes (so DSB can hold at most 1536 micro-ops in total). Based on our reverse engineering of multiple Intel processors shown in Table I, we find that when there is only one software thread running on the hardware core, address bits $addr[4:0]$ are used as the byte offset within the 32-byte window, and $addr[9:5]$ are the set index bits.

However, when two threads run in a hyper-threading setting on the same physical core, the set index bits are selected by an undocumented hash function. Through further investigation with micro-benchmarks, we reverse-engineered that the hash function does not use bits $\{10, 14, 16, 24\}$ of the virtual address. Thus if instruction addresses are only different in these 4 bit positions, they will map to the same DSB set. This can be used to generate collisions and evictions from the DSB.

TABLE I: Specifications of the tested Intel CPU models.

Model	Gold 6226	Xeon E-2174G	Xeon E-2286G	Xeon E-2288G
Microarchitecture	Cascade Lake	Coffee Lake		
Core Numbers	12	4	6	8
Thread Numbers	24	8	12	8 ^a
L1D configuration	32KB, 8-way, 64 byte line size, 64 sets			
DSB configuration	8-way, 32 byte window, 32 sets			
LSD entries	64	64 ^b	64 ^b	64
Frequency	2.7GHz	3.8GHz	4.0GHz	3.7GHz
OS	18.04 Ubuntu			
SGX Support	No	Yes		

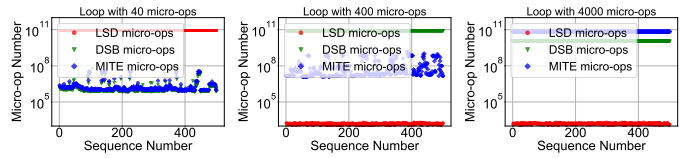
^aWe use Xeon E-2288G on Microsoft Azure cloud, this processor model is specific for Microsoft Azure and has hyper-threading disabled, although hyper-threading is supported by other E-2288G processors. ^bLSD is disabled in these machines.

3) *Validating Source of Observed Frontend Timing Differences:* To validate the timing changes observed are indeed due to different execution paths used, we performed a set of experiments which access $\{40, 400, 4000\}$ *mov* instructions in a loop that is repeated $\{2000 \text{ million}, 200 \text{ million}, 20 \text{ million}\}$ time, respectively (so that regardless the loop size all experiments execute in total 80 billion *mov* instructions). The loop with 40 micro-ops will directly use LSD (if it is enabled in the processor) since 40 micro-ops is within the 64 micro-op limit of the LSD capacity. The loop with 400 micro-ops will not be able to use LSD due to the loop size and force processing of the micro-ops in the DSB. Since the capacity of DSB (1536 micro-ops) is enough to hold 400 micro-ops from the loop, the MITE is disabled to conserve power. The loop with 4000 micro-ops will force the use of both LSD and MITE since the DSB can hold some (up to 1536) micro-ops, while extra micro-ops go through MITE. We did not find a way to force the use of MITE only, thus the three possible paths are using LSD (for small loops), DSB (for medium loops), and MITE+DSB (for large loops).

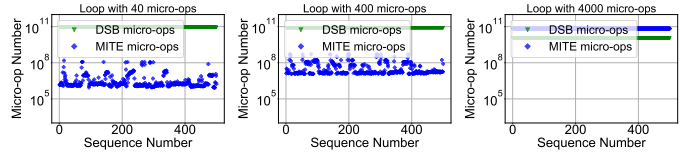
The histograms of the timing distributions, measured in cycles per micro-op, are shown in Figure 2.¹ The results are averages of 500 executions of our experiments, and we evaluated them on 4 machines: Intel Xeon Gold 6226, Intel Xeon E-2174G, Intel Xeon E-2286G, and Intel Xeon E-2288G. Configurations of the machines are shown in Table I. For the machines we tested, Figure 2 clearly shows differentiable timing distributions depend on which path is taken.

To verify the timing changes are indeed due to different frontend paths used for micro-op delivery, we use Linux `perf` tools [8] to measure the total number of micro-ops delivered by MITE, DSB, and LSD for loops with different number of micro-ops. The representative results from two machines are

¹Note that in Figure 2 we observe that DSB may have faster timing than the LSD, which correlates with the LSD’s purpose to save power. Power related attacks are discussed on Section VI. Also, for the machines that have disabled LSD, micro-ops will be naturally processed by DSB instead of LSD. Timing difference can still be observed for these machines for DSB vs. MITE timing.



(a) Intel Xeon Gold 6226 CPU



(b) Intel Xeon E-2174G CPU (LSD disabled)

Fig. 3: Performance counter readings for the different experiments, with small loops LSD (if present) indeed services the most micro-ops, for medium loops DSB handles most micro-ops, and for largest loops both MITE and DSB handle most micro-ops; this confirms that the experiments correctly trigger the different paths – and that resulting timing is related to the paths used.

shown in Figure 3.² It can be clearly seen that for Gold 6226 processor, when looping with 40 and 400 micro-ops, most of the micro-ops are processed by LSD and DSB, respectively. When looping with 4000 micro-ops, most of micro-ops are processed by both MITE and LSD. LSDs of E-2174U and E-2286U are disabled but the DSB and MITE processing differences are still clearly observable between loops with 400 and 4000 micro-ops. Micro-op delivery numbers of MITE also differ between loops with 40 and 400 micro-ops. Real attackers would not have access to these counters. We shown these only to validate our findings.

4) *Ensuring Observability of Frontend Timing:* When the DSB is used for instruction delivery, it can process at most 32 bytes or 6 micro-ops per cycle. However, the Register Alias Table (RAT) and retirement unit in the backend can only process 4 micro-ops per cycle at most. Therefore the maximum IPC is hard-limited to be 4 by the rename and retire unit, if we do not count the instruction fusion case.

Because the issue-widths of the frontend and the backend are not identical, in order to be able to observe any timing or power changes due to the frontend, one needs to carefully set up the instruction mix used to make sure the instruction delivery of frontend is the bottleneck.

For example, Intel Skylake has 8 execution ports in the backend to process micro-ops, but each port can only processes certain types of of micro-ops. Also, a DSB line will be ended by a branch instruction or a complex instruction even if the instruction stream does not entirely fill the DSB line. This also posts restrictions on the instruction mix that can be used to create bottlenecks in the frontend.

To achieve the best possible backend throughput and make the frontend bottleneck more significant, we found that the combination of 4 simple *mov* operations followed by 1 *jmp*

²Performance counters are disabled for Intel Xeon E-2288G processor in Microsoft Azure, so counter data is not shown. Intel Xeon E-2286G CPU performance number results are similar to Intel Xeon E-2174G CPU, so only counter data for E-2174G is shown.

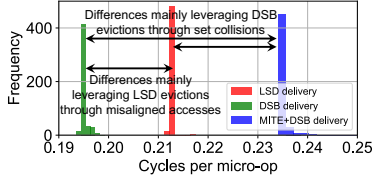


Fig. 4: Example histogram from Intel Xeon Gold 6226 processor of the timing distributions of using LSD, DSB, or MITE+DSB paths. Timing difference between LSD/DSB and MITE+DSB are used for collision-based attacks (see Section IV-A) and differences between LSD and DSB paths are used for misalignment-based attacks (see Section IV-B).

works the best in our tested processors. We do not want to touch data-related operations such as load and store because memory system will cause more unpredictable and larger timing difference which is not due to frontend path changes, and it would probably leave traces in the caches. The final instruction mix sequence which maximizes the timing signature of the frontend for our attacks should satisfy the following three requirements:

- Total byte size of one access block should not exceed 32 byte window (4 *mov* and 1 *jmp* use in total 25 bytes).
- Total micro-op number should not exceed 6 micro-op limit that DSB can process by one DSB line (4 *mov* and 1 *jmp* are decoded to total 5 micro-ops).
- Avoid port contention. The 4 *mov* instructions exploit the ports as much as possible, plus 1 *jmp* instruction to end the cache line block, while avoiding load, store, or more complex instructions involved, which will cause influence or noise from other microarchitectural units.

As the result, 4 *mov* plus 1 *jmp* sequence is the *instruction mix block* which fits the requirement, but other sequences using different instructions are possible.³

5) *Exploiting Frontend Path Timing Differences*: As can be seen from sample histogram from Intel Xeon Gold 6226 processor, shown in Figure 4, the timing difference of processing using DSB vs. MITE+DSB or LSD vs. DSB are clearly visible. Later we will use DSB vs. MITE+DSB timing differences to perform attacks related to DSB evictions through set collisions. On the other hand, the timing difference of processing using LSD vs. DSB will be used to perform attacks related to LSD evictions through misaligned accesses. Both of these also have power differences that separately can be used for power-based attacks.

B. Generating DSB Evictions Through Set Collisions

To force frontend path changes, we set up a series of instruction mix blocks and align the start of the instruction address of each block to map to the same DSB set, as shown in Figure 5. We make the *jmp* instructions at the end of each instruction mix block jump to the first instruction of next instruction mix block. In this case, executing the first *mov*

³An instruction mix block can be seen similarly as a gadget in speculative attacks, but we avoid using the term gadget since our vulnerabilities are not speculative execution vulnerabilities.

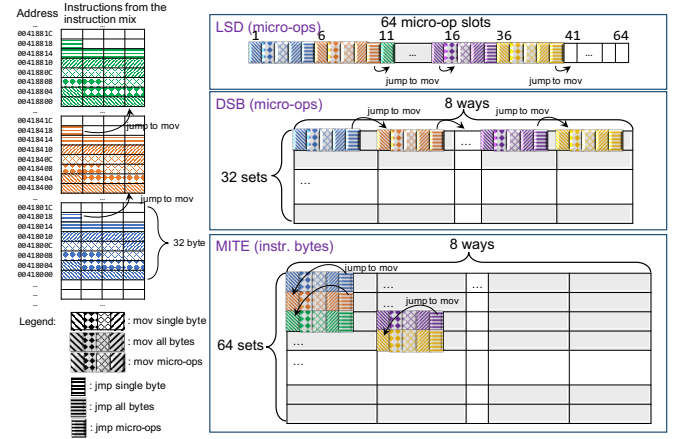


Fig. 5: Example of mapping instruction mix blocks (Section III-A4) to MITE, DSB, and LSD. Each instruction mix block is 5 micro-ops (4 *mov* plus 1 *jmp*). If number of chained 5 micro-op blocks is 8 then all will fit in LSD (since $8 \times 5 = 40 < 64$ micro-op limit of LSD) and they can all map to same DSB set (since DSB is 8-way associative).

instruction of the first instruction mix block will trigger a series of instruction mix block execution. If the chain of instruction mix blocks is less than 12, all the blocks should fit in LSD. However, at the same time, each DSB set has 8 ways, so 8 blocks can map to same set. Consequently, if the chain of blocks is set to 8 (rather than 12), they can both fit in LSD and same DSB set. But, as soon as the chain is extended to 9 (or more) blocks that map to same set, eviction occurs in DSB, and in turn force LSD eviction due to inclusive nature of MITE, DSB, and LSD.

Inclusive feature of MITE, DSB, and LSD means that eviction of lines from DSB will cause flush of the LSD unit. Furthermore, eviction from DSB redirects micro-ops to be processed by MITE. Combing these, eviction from DSB will cause transition of micro-op delivery from LSD to both DSB and MITE.

Note that changing the chain of instruction mix blocks from 8 to 9 will not cause eviction or misses of L1I cache. L1I caches for the machines we tested are 8-way associative and contain 64 sets of 64 bytes. Consequently, the size of the L1I is 4 times of DSB and instruction mix blocks mapping to the same DSB set will be mapped to different L1I sets, as is shown in Figure 5. In other words, changing chain length from 8 to 9 causes DSB and LSD eviction, but causes no misses in L1I.

C. Generating LSB Evictions Through Misaligned Accesses

We further found that misaligned instructions will generate collisions in the LSD, even when the number of total accessed instruction mix blocks does not exceed the DSB way number. This can be achieved by setting up the initial addresses of instruction mix blocks to be misaligned, for example, by aligning them on 8 byte boundaries that are not multiple of 32 bytes.

The alignment or misalignment of the blocks will cause different frontend path changes when processing micro-ops. When all the instruction mix blocks are misaligned, executing 4 chained instruction mix blocks that map to the same DSB

set will trigger collisions in LSD which causes the micro-op delivery change from LSD to DSB. At the same time, as we discussed in Section III-B, executing 4 chained instruction mix blocks that map to the same DSB set will use LSD unit since the size of the 4 blocks (of 5 micro-ops each) is less than 64 micro-op limit of the LSD.

When considering accessing both aligned and misaligned instructions, if accessing a chain of 7 instruction mix blocks which are all aligned, the 8th access will determine the path used. If the 8th access is aligned, all of the micro-ops will still be processed by the LSD. While if the 8th instruction mix block is misaligned, LSD will be flushed and micro-ops will be redirected to use DSB in the frontend. We found that {aligned + misaligned} instruction mix block access pairs that will cause micro-ops to be changed from the LSD to the DSB paths are: {5 aligned + 2 misaligned}, {6 aligned + 2 misaligned}, {3 aligned + 3 misaligned}, {4 aligned + 3 misaligned}, and {5 aligned + 3 misaligned}. Similar to DSB evictions, misalignment will not cause L1I cache misses.

IV. MICRO-OP CACHES AND PROCESSOR FRONTEND VULNERABILITIES

The vulnerabilities presented in this paper result in number of different new covert-channels that can be used for attacks. In this section, we focus on timing-based channels and attacks. Power-based channels and attacks are discussed in Section VI. Meanwhile, application of the channels to attack SGX enclaves is presented in Section VII, and for use with Spectre attacks in Section VIII. In addition, all the attack variants can be further differentiated based on the two techniques used to covertly send different bits by switching between different frontend paths: using eviction (following ideas in Section III-B) and using misalignment (following ideas in Section III-C). Regardless of the approach, there are three steps for all the attacks:

- **Initialization Step:** A series of instruction accesses are performed in this step to set the micro-ops into certain frontend paths.
- **Encoding Step:** The sender will access certain instructions to change frontend paths of micro-ops previously set in the initialization step according to the secret bit that is to be sent.
- **Decoding Step:** The same instructions accessed in the initialization step will be accessed again and final timing (or power) is measured.

A. Eviction-Based Timing Attacks in Multi-Threading (MT) Setting

For the eviction-based attacks, we deploy a sender thread and a receiver thread on a same physical processor core, but different hardware threads, which causes them to share the frontend. When the instruction stream from the sender conflicts in the same DSB set as the receiver's instruction stream, the receiver's instructions will be evicted from DSB, further triggering eviction from LSD so that the delivery of instructions falls back from the LSD to DSB+MITE, therefore generating detectable timing signature that the receiver can measure. This process leaves no interference in traditional instruction and

Algorithm 1: One iteration of eviction-based or misalignment-based covert transmission of 1 message bit

line 0– N : instruction lines mapping to the target set x or set y
 N : number of ways in the DSB
 m : a 1-bit message to transfer on the channel
 d : parameters of the receiver, $d < N + 1$
 M (only used for misalignment-based attacks): parameters of the receiver, $M < N + 1$

Step 1: Initialization:

Method 1 (Receiver):

```
for  $i = 0; i < d; i = i + 1$  do
  | Execute instruction line  $i$  mapping to set  $x$ ;
end
```

Sleep; // To allow the sender code to run here for encoding

Method 2:

(Receiver): Start the timer or power measurement and sleep;

// To allow encoding

```
for  $i = 0; i < d; i = i + 1$  do
```

```
  | (Sender): Execute instruction line  $i$  mapping to set  $x$ ;
```

```
end
```

Step 2: Encoding (Sender):

Eviction-based:

```
if  $m=1$  then
```

```
  for  $i = d; i < N + 1; i = i + 1$  do
    | Method 1,2: Execute instruction line  $i$  that maps to set  $x$ ;
  end
```

```
else
```

Method 1:

```
for  $i = d; i < N + 1; i = i + 1$  do
```

```
  | Execute instruction line  $i$  that maps to set  $y$ ;
```

```
end
```

Method 2: Do not execute instruction line

```
end
```

Misalignment-based:

```
if  $m=1$  then
```

```
  for  $i = d; i < M; i = i + 1$  do
```

```
    | Method 1,2: Execute misaligned instruction line  $i$  that maps to set  $x$ ;
```

```
  end
```

```
else
```

Method 1:

```
for  $i = d; i < M; i = i + 1$  do
```

```
  | Execute aligned instruction line  $i$  that maps to set  $x$ ;
```

```
end
```

Method 2: Do not execute instruction line

```
end
```

Step 3: Decoding:

Method 1 (Receiver):

```
for  $i = 0; i < d; i = i + 1$  do
```

```
  | Execute instruction line  $i$  mapping to set  $x$ ;
```

```
end
```

Collect time or power measurement for Step 3;

Method 2:

```
for  $i = 0; i < d; i = i + 1$  do
```

```
  | (Sender): Execute instruction line  $i$  mapping to set  $x$ ;
```

```
end
```

(Receiver): Collect time or power measurement for Steps 1-3;

data cache, and does not depend on speculation. Next we demonstrate two variants for the eviction-based attacks.

1) *MT Fast Eviction-Based Attack:* In this attack, the sender and the receiver first agree on the target instructions and DSB set x they will use to transfer information. The sender and the

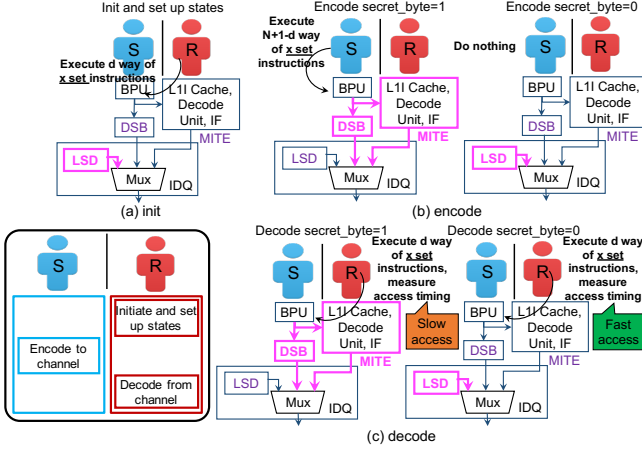


Fig. 6: Overview of the MT Fast Eviction-Based Attack.

receiver use in total $N + 1$ instruction mix blocks, denoted as lines $0 - N$, as discussed in Section III-A4, where N is the number of DSB ways. How the blocks are executed depends on the secret m 1-bit message that is to be sent. Further, d is a parameter used by the receiver to determine the different number of blocks used for each step. p is the number of iterations the receiver requires for initialization and decoding step for one timing measurement. q is the number of iterations the sender requires for encoding step. When sending each bit m of message, in order to reliably observe timing result with low error rate the initialize, encode, and decode steps need to be iterated for certain times accordingly.

For the MT Fast Eviction-Based Attack shown in Figure 6, in Step 1, the receiver executes the priming instructions, which correspond to Method 1 of Step 1 in Algorithm 1. In this step, d ($d \leq N$) instruction mix blocks that map to same DSB set x are accessed and it will iterate p times. In Step 2, the sender will execute different instruction series according to the secret bit m . When sending $m = 1$, the sender will execute $N + 1 - d$ instruction mix blocks q times that map to DSB set x . In this case, the total ways accessed is larger than N , which causes eviction of DSB and directs the micro-op delivery from LSD to DSB and MITE. When sending $m = 0$, the sender does nothing as is shown in Method 2 of Step 2 in Algorithm 1. Without conflicting in the DSB and the total number of micro-ops processed not exceeding LSD's limit, all the micro-ops will still be delivered by the LSD. In Step 3, the receiver will access the same d blocks accessed in Step 1 and time Step 3's access p times. If eviction happened, receiver's micro-ops in Step 3 will be delivered from DSB and MITE, where longer timing will be measured, indicating message $m = 1$ was sent from the sender. On the other hand, if no conflicts happen, receiver's micro-ops in step 3 will still be delivered from LSD, where much shorter timing is derived compared to MITE+DSB path, indicating message $m = 0$ is sent from the sender.

Take $d = 6$ and $N = 8$ for example (note that parameter M is not used for eviction-based attacks), the instruction access sequence when sending $m = 1$ and $m = 0$ are as follows:

- **Init.:** access blocks 1–6 mapping to set x
- **Encode:** access blocks 7–9 mapping to set x (if $m = 1$);

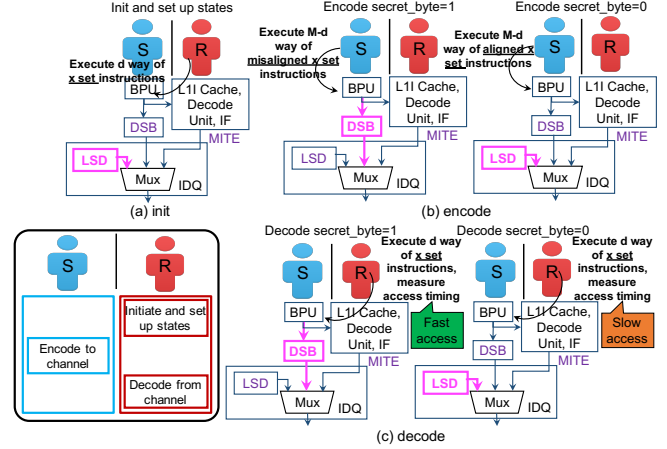


Fig. 7: Overview of MT Stealthy Misalignment-Based Attack.

no access (if $m = 0$)

- **Decode:** access blocks 1–6 mapping to set x (if $m = 1$, DSB and MITE are used; if $m = 0$, LSD access is used)

2) *MT Stealthy Eviction-Based Attack:* In a more stealthy case, to transmit $m = 1$, the sender executes $N + 1 - d$ instruction mix blocks q times that map to DSB set x . When transmitting $m = 0$, the sender can choose to execute the same number blocks q times as in the $m = 1$ case, but map them to a different DSB set. In this case, the channel is less reliable but the same number of instruction mix blocks $N + 1 - d$ are accessed for both sending 0 and 1, making the attack more stealthy considering monitoring of number of executed instructions, for example. This case corresponds to Method 1 of Step 2 shown in Algorithm 1.

Take $d = 6$ and $N = 8$ for example, the instruction access sequence when sending $m = 1$ and $m = 0$ are as follows:

- **Init.:** access blocks 1–6 mapping to set x
- **Encode:** access blocks 7–9 mapping to set x (if $m = 1$); 7–9 of set y (if $m = 0$)
- **Decode:** access blocks 1–6 mapping to set x (if $m = 1$, DSB and MITE are used; if $m = 0$, LSD access is used)

B. Misalignment-Based Attacks in Multi-Threading (MT) Setting

Misalignment mentioned in Section III-C can be used as covert channels as well. To achieve misaligned instruction access, sender and receiver first find virtual addresses of instructions that map to the same target set as what eviction-based attacks do, and then offset the initial address of every instruction mix blocks with 16 bytes to misalign the address. The offset byte numbers can be others while we choose half of the DSB line size 16, hence we select 16.

For this type of attacks, the total number of instruction mix blocks of the sender and the receiver are equal to or less than N ways of the DSB, which is an advantage as it reduces the accesses and increases the transmission rate compared with eviction-based attacks.

1) *MT Stealthy Misalignment-Based Attack:* The attack is shown in Figure 7. Here, the sender and the receiver use in

total M ($M \leq N$) instruction mix blocks. In Step 1 and Step 3, the receiver will access in total $p \times d$ (where $d < N$) sets of instructions mix blocks that map to one DSB set, which correspond to *Method 1* of Step 1 and Step 3 in Algorithm 1. In this case, the receiver’s instructions accessed in Step 1 will be processed by the LSD. For the sender, in Step 2, when sending $m = 1$, the sender will execute $(M - d)$ (where $M < N + 1$) sets of misaligned instructions that map to the same DSB set as the receiver for q times. In this case, misalignment of DSB causes the micro-op delivery to be redirected to DSB from LSD along with the aligned instruction access of the receiver, which leads to faster access of receiver’s instruction in Step 3. When sending $m = 0$, the sender will execute $(M - d)$ sets of instructions that map to the same DSB set for q times. The sets are aligned with the receiver’s instruction accesses, where the total number of ways accessed does not exceed the DSB’s N way number. In this case, all the micro-ops will still be delivered by the LSD and the receiver’s instruction access in Step 3 will derive slower access. This corresponds to *Method 1* of Step 2 in Algorithm 1.

Take $d = 5, N = 8, M = 8$ for example, the instruction access sequence when sending $m = 1$ and $m = 0$ are as follows:

- **Init.:** access blocks 1 – 5 mapping to set x
- **Encode:** access *misaligned* blocks 6 – 8 mapping to set x (if $m = 1$); *aligned* blocks 6 – 8 mapping to set x (if $m = 0$)
- **Decode:** access block 1 – 5 mapping to set x (if $m = 1$, DSB access is used; if $m = 0$, LSD access is used)

2) *MT Fast Misalignment-Based Attack:* Similarly to the eviction-based attacks, to achieve a faster version of the misalignment-based attack, in Step 2, the sender can choose to not execute any instruction lines when sending 0, as is shown in *Method 2* of Step 2 in Algorithm 1.

Take $d = 5, N = 8, M = 8$ for example, the access sequence when sending $m = 1$ and $m = 0$ are as follows:

- **Init.:** access access blocks 1 – 5 mapping to set x
- **Encode:** access *misaligned* blocks 6 – 8 mapping to set x (if $m = 1$); no access (if $m = 0$)
- **Decode:** access blocks 1 – 5 mapping to set x (if $m = 1$, DSB access is used; if $m = 0$, LSD access is used)

C. Attacks Not Requiring Multi-Threading (Non-MT)

Variants of the four types of fast or stealthy and eviction or misalignment attacks can be also created without using multi-threading; and they still work in cases where multi-threading may be disabled for security purposes. These attacks which do not leverage multi-threading, mainly require the sender to generate internal-interference to transmit secret bit information and the receiver externally measures the timing (or power, discussed later) of the sender’s execution to decode the information. Here we only demonstrate one type of attack not requiring multi-threading to show how the sender and the receiver behave. Three other types are possible, but are not discussed due to the limited space.

1) *Non-MT Stealthy Eviction-Based Attack:* This type of attack is shown in Figure 8. The number of iterations of sender’s encoding (q) and receiver’s initialization and decoding

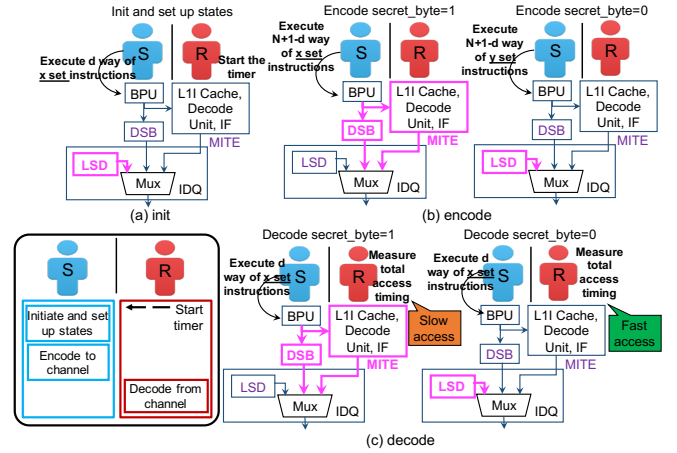


Fig. 8: Overview of Non-MT Stealthy Eviction-Based Attack.

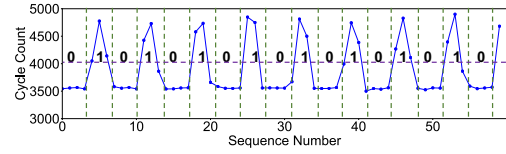


Fig. 9: Example trace of transmission of alternating 0s and 1s using the MT Fast Eviction-Based channel, with $d = 6$, and threshold being set to 4000 cycle count (purple dotted line).

(p) will be the sample in this attack ($p = q$). in order to reliably observe one timing result with low error rate. For one iteration, in Step 1, the receiver starts the timer in order to measure total time of the sender. The sender then executes d ($d \leq N$) sets of instructions mix blocks that map to DSB set x . This corresponds to *Method 2* of Step 1 in Algorithm 1 and instructions will be processed by the LSD. In Step 2, When sending $m = 1$, the sender will execute $N + 1 - d$ sets of instruction mix blocks that map to the same DSB set as the receiver. When sending $m = 0$, the sender will execute the same number of instructions but ones that map to a different DSB set y . This corresponds to *Method 1* of Step 2 in Algorithm 1. In Step 3, the sender will access the same d sets of instructions accessed in Step 1. Then the receiver will end the timer and calculate the total timing of the sender’s accesses to decode the information sent. If Step 2’s access maps to the same DSB set as Step 1 and eviction happens, sender’s micro-ops in Step 3 will be delivered from DSB and MITE, where longer timing will be measured, indicating $m = 1$ is sent from the sender. Otherwise, $m = 0$ is transmitted from the sender. This corresponds to *Method 2* of Step 3 in Algorithm 1.

V. EVALUATION

In this section, we evaluate the bit transmission rates and error rates of all the timing attacks discussed in Section IV. Power attacks, SGX attacks, and use of new covert channels in Spectre are evaluated later.

The evaluation is conducted on 4 recent x86_64 processors from Intel Skylake’s family. We list the specifications of the tested processor models in Table I. For testing each type of covert channel, the transmitted data is compared with the

TABLE II: Transmission rates and error rates of covert-channels when setting $d = 1$ for MT Fast Eviction-Based Attack for different message patterns: all 0s, all 1s, alternating 0s and 1s, and random.

	All 0s Message			All 1s Message			Alternating 0s and 1s Message			Random Message		
	G-6226	E-2174G	E-2286G	G-6226	E-2174G	E-2286G	G-6226	E-2174G	E-2286G	G-6226	E-2174G	E-2286G
Tr. Rate (Kbps)	42.66	49.53	87.33	55.28	61.17	102.39	50.21	58.86	64.96	18.28	21.80	25.61
Error Rate	0.00%	0.00%	0.00%	0.00%	0.00%	0.00%	2.68%	10.69%	12.56%	22.57%	18.53%	19.83%

TABLE III: Transmission rates and error rates of all the covert-channels when setting $d = 6$ for eviction-based attacks and $d = 5$, $M = 8$ for misalignment-based attacks. The transmitted message is alternating 0s and 1s. The bold transmission rates are the largest for the attacks. Intel Xeon E-2288G machine we tested has hyper-threading disabled so no data is shown for MT attacks for this machine..

	Non-MT Stealthy Eviction-Based				Non-MT Fast Eviction-Based				Non-MT Ste. Misalignment-Based				Non-MT Fast Misalignment-Based			
	G6226	2174G	2286G	2288G	G6226	2174G	2286G	2288G	G6226	2174G	2286G	2288G	G6226	2174G	2286G	2288G
Tr. Rate (Kbps)	419.67	851.81	1182.55	1356.43	501.06	977.68	1205.90	1399.96	713.01	466.02	723.15	1094.39	500.90	959.45	1228.35	1410.84
Error Rate	6.48%	3.43%	3.45%	0.36%	6.09%	0.00%	0.00%	0.00%	22.56%	11.34%	16.56%	10.08%	0.16%	0.00%	0.16%	0.00%

	MT Stealthy Eviction-Based				MT Fast Eviction-Based				MT Stealthy Misalignment-Based				MT Fast Misalignment-Based			
	G6226	2174G	2286G	2288G	G6226	2174G	2286G	2288G	G6226	2174G	2286G	2288G	G6226	2174G	2286G	2288G
Tr. Rate (Kbps)	37.20	97.62	114.62	—	115.97	113.02	161.63	—	41.61	122.93	139.13	—	129.36	152.44	200.37	—
Error Rate	26.26%	3.22%	2.52%	—	15.52%	14.44%	13.93%	—	32.98%	9.51%	9.81%	—	7.85%	2.77%	4.62%	—

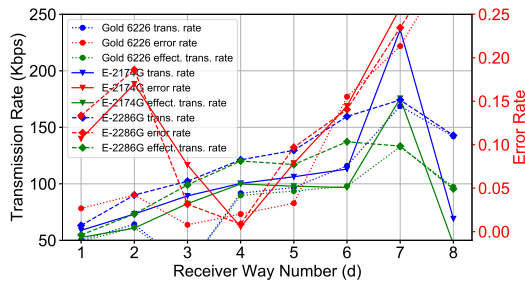


Fig. 10: Evaluation of MT Fast Eviction-Based Attack for different values of parameter d (receiver way number).

received data to compute the error rates. To evaluate the error rates of the channel, the Wagner-Fischer algorithm [23] is used to calculate the edit distance between the sent string and the received string.

A. Selecting Number of Iterations for Attack Steps

After careful tuning of the configurations, when sending each bit m of message, non-MT attacks can be reduced to set the iteration number $p = q = 10$ to repeat initialize, encode, and decode steps for reliably observing one timing result with low error rate. For each bit to transmit, the sender does one encoding step and receiver does one decoding step. For MT attacks, for each bit to transmit, the receiver repeats the decoding step at least 10 times (i.e., $p = 100$ while $q = 1000$) while the sender does one encoding step. Due to more noise in the MT setting, each bit has to be sent at least $p = 100$ times based on our experiments, compared to iteration $p = 10$ for the non-MT setting.

B. Selecting Threshold for Detecting Transmitted Bit ($m = 1$ vs. $m = 0$)

Example trace of transmission of alternating 1s and 0s is shown in Figure 9. To establish decoding threshold for timing measurements, an alternating pattern of 0s and 1s is sent, and the timing (measured in cycles using the `rdtscp` instruction) is averaged for 0s and 1s to establish the threshold. Based on different covert channels, if a measurement is 30 – 70% or

more above the threshold, it is judged to be a “1”, otherwise it is judged to be a “0”. The simple amplitude modulation encoding can be in future replaced with other channel coding methods [22] for possibly faster transmission.

C. Influence of (d, M) Transmission Parameters

To help find the ideal transmission rate, we evaluate the influence of d (number of ways accessed by the receiver) and its impact on the transmission rate and error rates.⁴ The results of changing d for MT Stealthy Eviction-Based Attack is shown in Figure 10. When increasing d from 1 to 8 (DSB has $N = 8$ sets), the number of ways accessed by the sender will decrease (number of sender’s ways accessed is $N + 1 - d$). Receiver’s observation will then become less stable (error rate increases) while on the other hand transmission rate increases. Error rates of small d (e.g., $d = 1, 2$) are also large because when the number of ways accessed by the receiver is small, timing difference of sending 0 and 1 is small which can be disrupted by the system noise. To find a balance between the transmission rate and error rate, we choose $d = 6$ for eviction-based attacks. For misalignment-based attacks, we choose $d = 5$, $M = 8$ (M is the total number of ways accessed by the sender and receiver for misalignment-based attacks, as can be seen in Algorithm 1).

To evaluate the impact of the transmitted message, we test the transmission for different message patterns: all 0s, all 1s, alternating 0s and 1s, and random. A sample evaluation of MT Stealthy Eviction-Based Attack for the four different message patterns with $d = 1$ is shown in Table II. From the results it can be seen that better transmission rate and error rate are derived for all 0s and all 1s. This is mainly because when not changing the bits (as is case for all 0s or all 1s), the frontend path used by the sender accesses remains the same, generating less noise. The random messages are the worst due to the frequent frontend path changes.

⁴This work is not aimed at achieving the highest bandwidth covert channel. To fully optimize the transmission rate and error rate, techniques such as the ones used in [27] can be further exploited.

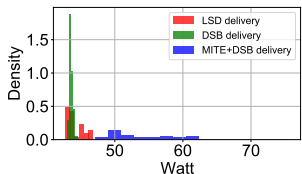


Fig. 11: Power histogram when choosing different frontend paths for machine Intel Xeon Gold 6226 CPU.

D. Transmission Rates and Error Rates

The bit transmission rates and error rates for all types of the timing-based attacks are presented in Table III, with $d = 6$ for eviction-based attacks and $d = 5$ for misalignment-based attacks. For the best attacks, the transmission rate can be as high as 1410 Kbps (1.41 Mbps) with almost 0% error rate.

In general, non-MT misalignment-based attacks have better transmission rate than the non-MT eviction-based attacks because non-MT misalignment-based attacks require fewer accesses (8 vs. 9) per loop iteration to transmit 1 bit of the message. Non-MT attacks have better transmission rate than MT attacks due to smaller noise that allows for faster transmission. On the other hand, the fast versions of the attacks have relatively higher transmission rates and lower error rates than stealthy-version counterparts. This is because the fast attacks use access vs. no access in the encode step, which creates more distinct timing differences.

VI. POWER-CHANNEL ATTACKS

The initial target for development of the DSB was not just performance but power. Processing micro-ops using DSB or LSD allows the whole MITE pipeline to turn off, resulting in noticeable power savings. In this case, switching between LSD or DSB and the MITE will not only cause timing change for instruction processing, but also power change, which is also used by our new attack variants. The power change can be measured by abusing unprivileged access to Intel’s Running Average Power Limit (RAPL) interface, which was introduced to ensure the CPU remains within desired thermal and power constraints [13].⁵ The RAPL has been recently abused by other security attacks [19].

Intel defines four different domains for RAPL [1]. We use power planes 0 (PP0) which contains the energy consumption estimates of the cores. In this way, the attack can directly access the sysfs interface and read the system file `/sys/devices/virtual/powercap/intel-rapl/intel-rapl:0/energy_uj` within the program to extract energy and derive the power value using the energy divided by user running time ($power = energy/time$). The timing is read from `rdtscp` instruction as in the timing-based attacks.

Figure 11 shows the histogram of the power consumption of utilizing different frontend paths for the micro-ops on the Gold 6226 processor. As can be seen, different frontend paths are differentiable by observing power changes.

⁵In power attacks, if unprivileged RAPL accesses are prevented, we can still use privilege access and use power to attack SGX enclaves. We do not show this type of attack due to the limited space.

TABLE IV: Power evaluation of Non-MT Attack on Gold 6226 CPU when setting $d = 6$ and input bit type to be alternation of 0s and 1s.

	Stealthy Eviction-Based	Stealthy Misalignment-Based
Tr. Rate (Kbps)	0.66	0.63
Error Rate	18.87%	9.07%

Power attacks are mostly effective for non-MT attacks since they experience less noise compared with the MT setting. Following the non-MT attack demonstrated in Section IV-C, we are able to detect LSD or DSB vs. MITE frontend path power difference caused by eviction or misalignment through observing the power change in RAPL. To observe the power differences, for each bit transmission the initialize, encode, and decode steps have to be iterated for $p = q = 240,000$ times since RAPL interface update interval is around 20kHz bandwidth [19], thus bandwidth of the power attacks is less than for the timing attacks.

Table IV shows the evaluation results of two non-MT attacks on Gold 6226 processor. The bandwidth of the power attacks is around 0.5 – 0.7 Kbps⁶ The transmission is still above 100 bps which is considered a high-bandwidth channel by the Trusted Computer System Evaluation Criteria (TCSEC) [24].

VII. ATTACKS ON SGX

The new vulnerabilities and the resulting covert channels can also be applied to attack SGX enclaves.

A. Overview of Intel SGX

The goal of Intel Software Guard Extension (SGX) is to protect sensitive data against the untrusted user, even on already compromised system, with the help of hardware implemented security and cryptographic mechanism inside the processor [1]. SGX allows the software developers to create encrypted enclaves containing secret data from banking apps or key wallets while retaining their confidentiality and integrity. The enclave’s data and code cannot be accessed from the outside and is protected from possibly malicious kernel or hypervisor at run-time. SGX provides numerous protections by disabling the performance counters to conceal the protected code, for example. This, however, means that any malicious or buggy code inside SGX will be difficult to find, and it can leak secrets from the enclave without easy detection.

This work focuses on SGX. The newer SGX2 extends SGX with dynamic memory management and other features. However, there are no SGX2 features that affect our attack, and thus we present our results on SGX, and they may be applicable to SGX2 as well.

B. SGX Attack Evaluation

The total execution timing of enclaves is not protected by SGX. Also, while the memory is protected, many other processor hardware resources still remain shared between enclave

⁶The power attack bandwidth can be further improved using techniques such as the ones shown in recent PLATUPUS work [19].

TABLE V: Transmission rates and error rates of covert-channels to attack SGX enclave when setting $d = 6$ for eviction-based attacks and $d = 5, M = 8$ for misalignment-based attacks. The transmitted message is alternating 0s and 1s. Intel Xeon E-2288G machine we tested has hyper-threading disabled so no MT attack data is provided for this machine.

SGX Attacks	Non-MT Stealthy Eviction-Based			Non-MT Fast Eviction-Based			Non-MT Ste. Misalignment-Based			Non-MT Fast Misalignment-Based		
	E-2174G	E-2286G	E-2288G	E-2174G	E-2286G	E-2288G	E-2174G	E-2286G	E-2288G	E-2174G	E-2286G	E-2288G
Tr. Rate (Kbps)	18.96	19.56	21.20	29.35	32.01	34.48	23.93	24.70	27.10	30.36	31.18	35.20
Error Rate	0.16%	1.33%	2.18%	0.04%	1.40%	0.40%	0.32%	0.76%	0.76%	0.08%	1.08%	0.68%

SGX Attacks	MT Stealthy Eviction-Based			MT Fast Eviction-Based			MT Stealthy Misalignment-Based			MT Fast Misalignment-Based		
	E-2174G	E-2286G	E-2288G	E-2174G	E-2286G	E-2288G	E-2174G	E-2286G	E-2288G	E-2174G	E-2286G	E-2288G
Tr. Rate (Kbps)	7.84	11.97	—	7.85	14.89	—	6.30	10.54	—	6.39	13.62	—
Error Rate	11.22%	10.20%	—	6.74%	8.02%	—	1.24%	0.52%	—	2.56%	12.95%	—

TABLE VI: Effective transmission rates and error rates of Spectre V1 Attack compared with other covert channels. Microsoft Azure does not enable `perf` tools so L1 miss rate is not able to measure in the Intel Xeon E-2288G machine. L1 miss rate from work [37] are all L1D miss rates.

	MEM F+R [37]	L1D F+R [37]	L1D LRU [37]	L1I F+R		L1I P+P		This Work	
				Gold 6226	E-2288G	Gold 6226	E-2288G	Gold 6226	E-2288G
Eff. Tr. Rate (Kbps)	—	—	—	0.035	0.047	0.038	0.049	0.332	0.578
L1 Miss Rate	2.81%	4.79%	4.48%	0.45%	—	0.48%	—	0.21%	—

and non-enclave code, including the processor frontend. Based on that, we develop different new attacks targeting SGX.

We implement an enclave that exploits an *ecall* function to encrypt a buffer using an in-enclave secret key. To demonstrate our attacks in an SGX environment, the sender trojan is running inside the SGX enclave and manipulates the use of the frontend paths to communicate to a receiver outside of the SGX.

1) *MT SGX Attacks*: For MT SGX attacks, the sender maintains its own thread and performs the covert transmission within the enclave. Meanwhile, the receiver decodes bits of the sender by measuring the timing of its own memory instructions. Under this scenario, if the frontend path components (MITE, DSB, and LSD) are shared between the enclave and non-enclave code, the receiver is able to detect the performance difference of its own instruction access when there are receiver’s micro-op delivery path changes due to the sender’s covert transmission within the enclave.

From Table V it can be seen that the transmission rates of MT SGX attacks can be roughly 6 Kbps – 15 Kbps with iteration numbers $p = 1,000, q = 10,000$, while maintaining the similar error rate as the MT non-SGX attacks.

2) *Non-MT SGX Attacks*: For non-MT SGX attacks, the sender trojan is still inside the enclave, while the receiver derives the information by measuring the timing of SGX operation from outside of the enclave. Under this scenario, the receiver’s observations depend on ability to detect the self-interference of the sender’s accesses within the enclave, to detect whether there are frontend path changes caused by the eviction or misalignment of the micro-ops or not. The non-MT SGX attacks, because they do not leverage multi-threading, are possible even when multi-threading is disabled for security reasons.

In the non-MT setup, the sender and receiver alternate executing on the same thread and core. To reduce overhead and noise of enclave exits and entrances, for each transmission of a bit, there is only one entrance and exit. Effectively the receiver starts time measurement, then allows the enclave to run, and then finally measures the timing of the enclave as it was affected by the frontend paths. Compared to non-SGX attacks,

more iterations of initialization, encoding, and decoding are necessary ($p = q = 1,000 - 5,000$ iterations for the SGX attack compared to $p = q = 10$ iterations for non-SGX attacks) in order to transmit one bit.

As Table V shows, the transmission rates of non-MT SGX attacks are roughly 1/25 to 1/30 of non-MT non-SGX attacks, while still maintaining acceptable and even lower error rates. Power-based attacks are also possible, but they would have lower transmission rates, and are not further discussed due to limited space.

VIII. NEW SPECTRE ATTACK VARIANT

Speculative attacks typically leverage transient execution to access secret and then a covert channel to pass the secret to the attacker [7], [18], [20]. Currently, most proof-of-concept codes of speculative attacks use the cache Flush+Reload [40] covert channel. In this section, we demonstrate that our new covert channels using processor frontend can also be applied to Spectre attacks to encode and decode the secret.

In our Spectre attacks, the secret message is represented by 5 bit chunks (each chunk can have value from 0 to 31). We then use each of the 32 DSB sets to represent each value. Similar to cache-based channels, during the speculative execution secret value is encoded by accessing the corresponding set. Unlike with cache attacks, to access a DSB set, instruction mix block mapping to that set has to be executed.

To help compare to Spectre with cache-based channels, we also implement Spectre attacks using L1I cache Flush + Reload attack and L1I Prime + Probe attack, to compare to covert-channels that all target on the instructions. To demonstrate the speculative attack, we modify the Spectre variant 1 attack sample code [18] to make the victim (sender) code to execute related instructions, and change the attacker (receiver) code to use the frontend channel, L1I Flush+Reload channel, and L1I Prime+Probe channel, respectively, as the disclosure primitives (instead the regular data cache primitives used in the original variant 1).

Table VI shows the transmission rate when using our channel compared to other channels. We highlight the L1 cache miss rate (including both the victim and the attacker)

during a Spectre attack for the three different covert channels and show the comparison results with L1 data (L1D) cache covert channels from [37]. Our data are derived from averaging 30 speculative attack runs.

Compared with L1D cache and LRU [37] covert channel which targets stealthy attacks without causing high data cache miss rate, instruction-based covert channels have even lower L1 cache miss rate in general. Apart from that, since our frontend attack does not require causing cache misses at all to perform the attacks, the L1 miss rate is even smaller compared with the other two L1I cache covert channels. Moreover, comparing to the L1I Flush+ Reload and L1I Prime+ Probe channel, the advantage of the frontend attack is the short encoding time of the sender, which leads to a smaller speculative window required and makes the attack more dangerous and harder to defend. This also results in higher effective transmission rate compared with other L1I cache channel. The transmission rate of frontend attack is around 750 bps, which is already considered a high-bandwidth channel by the Trusted Computer System Evaluation Criteria (TCSEC) [24].

IX. DISCUSSION

The vulnerabilities do not involve interference in traditional instruction or data caches, and they do not involve speculation. Therefore, a large set of existing defense mechanism will not be able to prevent them [17], [26], [39]. While it seems that simply partitioning the DSB or LSD would be a possible defense, partitioning the DSB or LSD would largely reduce the hit ratio of DSB and LSD, and therefore cause more LSD, DSB, and MITE switch penalties, which would make the pipeline even slower than without DSB and LSD, negating their benefits.

The major difficulty of dealing with the security vulnerabilities of the frontend paths is that the frontend is designed to give better performance or lower power for different execution scenarios, which inevitably creates inherent timing or power signatures. Eliminating these timing or power signatures would reduce the performance or power benefits. Since frontend components such as the MITE, DSB, and LSD are widely used in modern architecture designs. Defending the vulnerabilities will require new approaches for design of the frontend.

X. CONCLUSION

This paper demonstrated a new class of vulnerabilities rooted in the multiple paths in the processor frontend, and we demonstrated numerous covert channels based on the timing or power of the frontend components. This paper in particular showed for the first time that different frontend paths (MITE, DSB, or LSD) to process micro-ops can be abused to leak fine-grained information about victim process's activity by observing timing differences or power changes, and at the same time causing no misses in the L1 or lower caches, and with no need to introduce speculation. We demonstrated the threats to SGX as well using the frontend components, and used the covert channels to develop new variant of Spectre speculative execution attacks.

ACKNOWLEDGEMENT

Shuwen Deng was supported by a Google PhD Fellowship. This work was also supported in part NSF grant 1813797 and through SRC award number 2844.001. We thank Abhishek Bhattacharjee for his insightful comments and feedback.

REFERENCES

- [1] "Intel 64 and ia-32 architectures software developer's manual: Volume 3," <https://www.intel.com/content/www/us/en/architecture-and-technology/64-ia-32-architectures-software-developer-system-programming-manual-325384.html>.
- [2] "Snoop-assisted L1 data sampling," <https://software.intel.com/security-software-guidance/advisory-guidance/snoop-assisted-l1-data-sampling>.
- [3] A. C. Aldaya, B. B. Brumley, S. ul Hassan, C. P. García, and N. Tuveri, "Port contention for fun and profit," in *2019 IEEE Symposium on Security and Privacy (SP)*. IEEE, 2019, pp. 870–887.
- [4] D. J. Bernstein, "Cache-timing attacks on aes," 2005.
- [5] A. Bhattacharyya, A. Sandulescu, M. Neugschwandtner, A. Sorniotti, B. Falsafi, M. Payer, and A. Kurmus, "Smotherspectre: exploiting speculative execution through port contention," in *Conference on Computer and Communications Security*, 2019, pp. 785–800.
- [6] C. Canella, D. Genkin, L. Giner, D. Gruss, M. Lipp, M. Minkin, D. Moghimi, F. Piessens, M. Schwarz, B. Sunar *et al.*, "Fallout: Leaking data on meltdown-resistant cpus," in *Proceedings of the 2019 ACM SIGSAC Conference on Computer and Communications Security*, 2019, pp. 769–784.
- [7] C. Canella, J. Van Bulck, M. Schwarz, M. Lipp, B. Von Berg, P. Ortner, F. Piessens, D. Evtvushkin, and D. Gruss, "A systematic evaluation of transient execution attacks and defenses," in *28th {USENIX} Security Symposium ({USENIX} Security 19)*, 2019, pp. 249–266.
- [8] A. C. De Melo, "The new linux perf tools," in *Slides from Linux Kongress*, vol. 18, 2010, pp. 1–42.
- [9] S. Deng and J. Szefer, "New predictor-based attacks in processors," in *Proceedings of the Design Automation Conference*, ser. DAC, December 2021.
- [10] D. Evtvushkin, D. Ponomarev, and N. Abu-Ghazaleh, "Jump over aslr: Attacking branch predictors to bypass aslr," in *2016 49th Annual IEEE/ACM International Symposium on Microarchitecture (MICRO)*. IEEE, 2016, pp. 1–13.
- [11] D. Evtvushkin, R. Riley, N. C. Abu-Ghazaleh, ECE, and D. Ponomarev, "Branchscope: A new side-channel attack on directional branch predictor," *ACM SIGPLAN Notices*, vol. 53, no. 2, pp. 693–707, 2018.
- [12] C. Gongye, Y. Fei, and T. Wahl, "Reverse-engineering deep neural networks using floating-point timing side-channels," in *2020 57th ACM/IEEE Design Automation Conference (DAC)*. IEEE, 2020, pp. 1–6.
- [13] C. Gough, I. Steiner, and W. Saunders, *Energy efficient servers: blueprints for data center optimization*. Springer Nature, 2015.
- [14] B. Gras, K. Razavi, H. Bos, and C. Giuffrida, "Translation leak-aside buffer: Defeating cache side-channel protections with {TLB} attacks," in *27th {USENIX} Security Symposium ({USENIX} Security 18)*, 2018, pp. 955–972.
- [15] D. Gruss, C. Maurice, A. Fogh, M. Lipp, and S. Mangard, "Prefetch side-channel attacks: Bypassing smap and kernel aslr," in *Proceedings of the 2016 ACM SIGSAC conference on computer and communications security*, 2016, pp. 368–379.
- [16] D. Gruss, C. Maurice, K. Wagner, and S. Mangard, "Flush+ flush: a fast and stealthy cache attack," in *International Conference on Detection of Intrusions and Malware, and Vulnerability Assessment*. Springer, 2016, pp. 279–299.
- [17] V. Kiriansky, I. Lebedev, S. Amarasinghe, S. Devadas, and J. Emer, "Dawg: A defense against cache timing attacks in speculative execution processors," in *2018 51st Annual IEEE/ACM International Symposium on Microarchitecture (MICRO)*. IEEE, 2018, pp. 974–987.
- [18] P. Kocher, J. Horn, A. Fogh, D. Genkin, D. Gruss, W. Haas, M. Hamburg, M. Lipp, S. Mangard, T. Prescher *et al.*, "Spectre attacks: Exploiting Speculative Execution," in *Symposium on Security and Privacy (S&P)*, 2019, pp. 1–19.
- [19] M. Lipp, A. Kogler, D. Oswald, M. Schwarz, C. Easdon, C. Canella, and D. Gruss, "Platypus: Software-based power side-channel attacks on x86," in *IEEE Symposium on Security and Privacy (SP)*, 2021.

- [20] M. Lipp, M. Schwarz, D. Gruss, T. Prescher, W. Haas, A. Fogh, J. Horn, S. Mangard, P. Kocher, D. Genkin *et al.*, “Meltdown: Reading kernel memory from user space,” in *27th {USENIX} Security Symposium ({USENIX} Security 18)*, 2018, pp. 973–990.
- [21] F. Liu, Y. Yarom, Q. Ge, G. Heiser, and R. B. Lee, “Last-level cache side-channel attacks are practical,” in *2015 IEEE symposium on security and privacy*. IEEE, 2015, pp. 605–622.
- [22] J. L. Massey, “Foundation and methods of channel encoding,” in *Proc. Int. Conf. Information Theory and Systems*, vol. 65. NTG-Fachberichte, 1978, pp. 148–157.
- [23] G. Navarro, “A guided tour to approximate string matching,” *ACM computing surveys (CSUR)*, vol. 33, no. 1, pp. 31–88, 2001.
- [24] “DoD 5200.28-STD, Department of Defense Trusted Computer System Evaluation Criteria,” 1983, <http://csrc.nist.gov/publications/history/dod85.pdf>.
- [25] R. Paccagnella, L. Luo, and C. W. Fletcher, “Lord of the ring (s): Side channel attacks on the cpu on-chip ring interconnect are practical,” *arXiv preprint arXiv:2103.03443*, 2021.
- [26] M. K. Qureshi, “Ceaser: Mitigating conflict-based cache attacks via encrypted-address and remapping,” in *2018 51st Annual IEEE/ACM International Symposium on Microarchitecture (MICRO)*. IEEE, 2018, pp. 775–787.
- [27] G. Saileshwar, C. W. Fletcher, and M. Qureshi, “Streamline: A fast, flushless cache covert-channel attack by enabling asynchronous collusion,” 2021.
- [28] M. Schwarz, M. Lipp, D. Moghimi, J. Van Bulck, J. Stecklina, T. Prescher, and D. Gruss, “Zombieload: Cross-privilege-boundary data sampling,” in *Proceedings of the 2019 ACM SIGSAC Conference on Computer and Communications Security*, 2019, pp. 753–768.
- [29] M. Schwarz, M. Schwarzl, M. Lipp, J. Masters, and D. Gruss, “Netspectre: Read arbitrary memory over network,” in *European Symposium on Research in Computer Security*. Springer, 2019, pp. 279–299.
- [30] D. Skarlatos, M. Yan, B. Gopireddy, R. Sprabery, J. Torrellas, and C. W. Fletcher, “Microscope: enabling microarchitectural replay attacks,” in *2019 ACM/IEEE 46th Annual International Symposium on Computer Architecture (ISCA)*. IEEE, 2019, pp. 318–331.
- [31] C. Trippel, D. Lustig, and M. Martonosi, “Meltdownprime and Spectreprime: Automatically-Synthesized Attacks Exploiting Invalidation-Based Coherence Protocols,” *arXiv preprint arXiv:1802.03802*, 2018.
- [32] J. Van Bulck, M. Minkin, O. Weisse, D. Genkin, B. Kasikci, F. Piessens, M. Silberstein, T. F. Wenisch, Y. Yarom, and R. Strackx, “Foreshadow: Extracting the keys to the intel {SGX} kingdom with transient out-of-order execution,” in *27th {USENIX} Security Symposium ({USENIX} Security 18)*, 2018, pp. 991–1008.
- [33] J. Van Bulck, D. Moghimi, M. Schwarz, M. Lipp, M. Minkin, D. Genkin, Y. Yuval, B. Sunar, D. Gruss, and F. Piessens, “LVI: Hijacking Transient Execution through Microarchitectural Load Value Injection,” in *41th IEEE Symposium on Security and Privacy (S&P’20)*, 2020.
- [34] S. van Schaik, A. Milburn, S. Österlund, P. Frigo, G. Maisuradze, K. Razavi, H. Bos, and C. Giuffrida, “RIDL: Rogue in-flight data load,” in *S&P*, May 2019.
- [35] Y. Wang, A. Ferraiuolo, and G. E. Suh, “Timing channel protection for a shared memory controller,” in *2014 IEEE 20th International Symposium on High Performance Computer Architecture (HPCA)*. IEEE, 2014, pp. 225–236.
- [36] O. Weisse, J. Van Bulck, M. Minkin, D. Genkin, B. Kasikci, F. Piessens, M. Silberstein, R. Strackx, T. F. Wenisch, and Y. Yarom, “Foreshadowing: Breaking the virtual memory abstraction with transient out-of-order execution,” 2018.
- [37] W. Xiong and J. Szefer, “Leaking information through cache lru states,” in *2020 IEEE International Symposium on High Performance Computer Architecture (HPCA)*. IEEE, 2020, pp. 139–152.
- [38] —, “Survey of transient execution attacks,” *ACM Computing Surveys*, 2021.
- [39] M. Yan, J. Choi, D. Skarlatos, A. Morrison, C. Fletcher, and J. Torrellas, “Invisispec: Making speculative execution invisible in the cache hierarchy,” in *2018 51st Annual IEEE/ACM International Symposium on Microarchitecture (MICRO)*. IEEE, 2018, pp. 428–441.
- [40] Y. Yarom and K. Falkner, “Flush+ reload: A high resolution, low noise, l3 cache side-channel attack,” in *23rd {USENIX} Security Symposium ({USENIX} Security 14)*, 2014, pp. 719–732.